NIH Public Access

Author Manuscript

Neuroimage. Author manuscript; available in PMC 2013 July 29.

Published in final edited form as:

Neuroimage. 2010 February 15; 49(4): 2995–3004. doi:10.1016/j.neuroimage.2009.10.015.

Altered White Matter Microstructure in the Corpus Callosum in Huntington's Disease: implications for cortical "disconnection"

H Diana Rosas, MD[1,2,3], **Stephanie Y Lee, BS**[1,2,3], **Alexander Bender, BS**[1,2,3], **Alexandra K Zaleta, EdM**[1,2,3], **Mark Vange, PhD**[3], **Peng Yu, PhD**[3,4], **Bruce Fischl, PhD**[3,4], **Vasanth Pappu, BS**[1,2,3], **Jang-Ho Cha, MD PhD**[1], **David H Salat, PhD**[2,3], and **Steven M. Hersch, MD PhD**[1]

[1]Department of Neurology, Massachusetts General Hospital and Harvard Medical School, Boston, MA

[2]Center for Neuroimaging of Aging and Neurodegenerative Diseases, Massachusetts General Hospital and Harvard Medical School, Charlestown, MA

[3]Athinoula A. Martinos Center for Biomedical Imaging, Massachusetts General Hospital/Harvard Medical School, Charlestown, MA

[4]Harvard-MIT Division of Health Sciences and Technology Massachusetts Institute of Technology, Cambridge, MA

Abstract

The corpus callosum (CC) is the major conduit for information transfer between the cerebral hemispheres and plays an integral role in relaying sensory, motor and cognitive information between homologous cortical regions. The majority of fibers that make up the CC arise from large pyramidal neurons in layers III and V, which project contra-laterally. These neurons degenerate in Huntington's disease (HD) in a topographically and temporally selective way. Since any focus of cortical degeneration could be expected to secondarily de-afferent homologous regions of cortex, we hypothesized that regionally selective cortical degeneration would be reflected in regionally selective degeneration of the CC. We used conventional T1-weighted, diffusion tensor imaging (DTI), and a modified corpus callosum segmentation scheme to examine the CC in healthy controls, huntingtin gene-carriers and symptomatic HD subjects. We measured mid-sagittal callosal cross-sectional thickness and several DTI parameters, including fractional anisotropy (FA), which reflects the degree of white matter organization, radial diffusivity, a suggested index of myelin integrity, and axial diffusivity, a suggested index of axonal damage of the CC. We found a topologically selective pattern of alterations in these measures in pre-manifest subjects that were more extensive in early symptomatic HD subjects and that correlated with performance on distinct cognitive measures, suggesting an important role of for disrupted inter-hemispheric transfer in the clinical symptoms of HD. Our findings provide evidence for early degeneration of commissural pyramidal neurons in the neocortex, loss of cortico-cortical connectivity, and functional compromise of associative cortical processing.

Address correspondence and reprint requests to: H. Diana Rosas, M.D. Center for Neuro-imaging of Aging and Neurodegenerative Diseases, 149 13th Street, Room 2275, Charlestown, MA 02129, Phone (617) 726-0658 Fax (617) 724-1227 rosas@helix.mgh.harvard.edu.

The authors have no financial interest in the research reported.

INTRODUCTION

Huntington's disease (HD) is a fatal, autosomal dominant disorder characterized clinically by involuntary movements, neuropsychiatric disturbances and cognitive decline. HD leads to a selective regional neurodegeneration in vulnerable populations of neurons in many regions of the brain. While the striatum has long been recognized for its involvement in HD, recent studies have demonstrated early and significant, neuropathology in the cerebral cortex and have suggested its involvement in important clinical features and progression (Rosas et al., 2008b). In the neocortex, neurodegeneration in HD especially involves layers III, V and VI (Hedreen et al., 1991). These layers are made up primarily of pyramidal neurons that give rise to long-reaching intra- and extracortical projections. Layer III pyramidal cells primarily give rise to long association fibers that connect intra-hemispheric cortical regions and to inter- hemispheric commissural fibers that project through the corpus callosum (CC) (Sach et al., 2004). With the exception of a few of studies that used whole-brain approaches to evaluate white matter changes, the CC has been largely unexamined in HD (Douaud et al., 2009; Kloppel et al., 2008; Lange et al., 1976; Reading et al., 2005; Rosas et al., 2006; Weaver et al., 2009). Because the CC plays a key role as the primary cortical projection system connecting the two brain hemispheres, and because cortical atrophy in HD is regionally and temporally selective, focal changes in the CC would be expected. Moreover, because regions of the CC reflect homotypically organized inter-hemispheric connections, damage to specific sub-regions might explain specific cognitive deficits in HD. Alterations in the CC, including changes in morphometry or in microstructure within the CC, have been reported in several neuropsychiatric disorders and neurological disorders including dementia (Salat et al., 2008; Stricker et al., 2009) multiple sclerosis (Lowe et al., 2006) and motor neuron disease, as well as in normal aging (Salat et al., 2005a); neurological and clinical symptoms of several of these disorders and may be related to altered connectivity. In each, some regions were more thinned or showed evidence of microstructural white matter changes than in others. While we have demonstrated callosal microstructural alterations in HD previously, a comprehensive evaluation of the changes that take place regionally has not been done. Since neurodegeneration is a slow process in HD in which neurites are remodeled and retract long before cell death, we hypothesized that alterations in the CC are likely to occur especially early, long before symptoms are present. We also hypothesized that progressive alterations in callosal functional connectivity might underlie some of the disabling symptoms of HD.

The CC is made up of densely packed, myelinated nerve fibers that primarily connect homologous regions of the cortex. These fibers remain topographically ordered as they pass through the CC (Innocenti, 1994) which facilitates the investigation of the CC using non-invasive neuro-imaging tools, such as diffusion tensor imaging (DTI). DTI provides information about the magnitude and direction of water diffusion within tissue (Pierpaoli et al., 2001) and provides measures to characterize the integrity of the microstructure of white matter fibers. Fractional anisotropy (FA) is a scalar measure that describes the coherence of oriented structures (Cercignani and Horsfield, 2001); intracellular water within myelinated axons diffuses in a more specifically directional manner as compared to diffusion in unmyelinated axons. Thus, high FA corresponds to preferential diffusion along one fiber orientation, indicating higher tissue organization (Schulte et al., 2005). Newer measures, focusing on directional diffusivity, include radial diffusivity, which is believed to reflect breakdown of the myelin sheath, and axial diffusivity, which may implicate axonal damage that would occur secondarily to Wallerian degeneration (Kim et al., 2006; Song et al., 2002). These diverse DTI measures may provide new insights into novel neuropathological mechanisms in even normal appearing brain regions (Pfefferbaum et al., 2008; Sun et al., 2003).

Our previous work has demonstrated early degeneration of sensori-motor and occipital cortical areas in individuals with HD (Rosas et al., 2002; Rosas et al., 2008b); we hypothesized that alterations in the CC would reflect the underlying regional and temporal changes in the cortex. We combined high-resolution T1-weighted imaging with quantitative DTI, including FA, axial and radial diffusivity, to investigate changes in cross-sectional thickness and microstructure along the medial axis of the CC throughout the spectrum from pre-manifest through early stages of HD. We evaluated changes along the entire stretch of a mid-sagittal skeleton that was generated as well as changes in five distinct anatomical regions, based on anatomical and functional connectivity between cortical areas as proposed by Hofer et al (Hofer and Frahm, 2006). This CC parcellation scheme has been used to study the CC in other neurodegenerative disorders and follows histological studies of callosal topography (Keshavan et al., 2002; Kim et al., 2008).

We hypothesized that the regional pattern of CC atrophy in Pre-HD and HD would correspond to region-specific cortical neurodegeneration, effectively resulting in commissural “disconnection” in HD. We also investigated the relationship between cross-sectional thickness and FA measures; we hypothesized that diffusion measures might have a greater sensitivity than morphometry since degenerative tissue changes likely occur prior to measurable CC atrophy, and would reflect early neuronal dysfunction, rather than neurodegeneration, in HD. Finally, we hypothesized that alterations in regional connectivity might contribute to cognitive dysfunction in HD.

METHODS

Subjects

Individuals with symptomatic HD (N=21, 8M/13F, mean age 46.4 ± 8.9) and those with the genetic expansion that causes HD but who were without motor symptoms (pre-manifest, PHD, N=19, 8M/13F mean age 40.2 ± 10.4) were recruited through the Massachusetts General Hospital (MGH) Movement Disorders Clinic. PHD and HD subjects were assessed by a neurologist from the Movement Disorders Clinic (HDR). PHD subjects had undergone pre-symptomatic genetic testing, which was diagnostic in all (CAG number ≥ 40). HD subjects had unequivocal motor symptoms and either a known family history of HD or a known trinucleotide repeat expansion. Age and gender-matched healthy adults for each group were recruited (N=19, 7M/12F, mean age 45.2 ± 8.7 HD-matched subjects; N=21 8M/13F mean age 39.7 ± 11.3 PHD-matched subjects) from the community. Procedures were fully explained to all individuals and written informed consent was obtained in accordance with the Human Research Committee guidelines of MGH. Protocols were performed in compliance with institutional guidelines provided by the Internal Review Board at MGH. All individuals were assessed with cognitive and functional components of the Unified Huntington’s Disease Rating Scale (UHDRS), including Stroop Color Word, Digit Symbol, and Verbal Fluency. To examine relationships between clinical and imaging measures and proximity to the predicted onset of HD symptoms, we used a CAG-based prognostic model as described previously (Langbehn et al., 2004). Within this group, subjects were divided at the group median for predicted years to expected onset, operationally defined as “near” to onset (N=10), less than 11 years to estimated diagnosis, and “far” from onset (N=11) onset, those greater than 11 years to expected diagnosis (N=10). Symptomatic HD subjects were stratified into two groups, those with a total functional capacity score of greater than 9 (HD1) and those between 7 and 9 (HD2). Characteristics of the study group are given in Table 1.

NIH-PA Author Manuscript

NIH-PA Author Manuscript

Data Acquisition and pre-processing

Imaging data were acquired on a 1.5T Siemens Avanto scanner (Erlangen Germany). *CC Morphometric analyses*: For the cross-sectional CC thickness measurements, two high-resolution MPRAGE scans were motion corrected and averaged for each subject (resolution 1.3 × 1 × 1.3 mm, TR = 2730 ms, TE = 3.31 ms, matrix 256 mm × 256 mm, slice thickness 1.33 mm, 128 slices, FA = 7°, T1 = 1000 ms) in order to create a single image volume with high contrast-to-noise. *CC DTI Analyses*: WM integrity was assessed using DTI measures of FA and diffusivity (comprised of axial and radial components) (Budde et al., 2007; Song et al., 2002; Song et al., 2005). Image acquisition employed a single shot echo planar imaging with a twice-refocused spin echo pulse sequence, optimized to minimize eddy current-induced image distortions as described previously and used in our prior work (Reese et al., 2003; Salat et al., 2008) (TR/TE = 7400/89 ms, b=700 s/mm^2, 256 mm × 256 mm FOV, 2 mm slice thickness, isotropic, with 0 mm gap, 10 T2 + 60 DWI, isotropic, 64 slices in the AC-PC plane). The 60 non-colinear directions were obtained using the electrostatic shell method (Jones et al., 1999), providing a high signal to noise diffusion volume.

Segmentation Algorithm—The inter-hemispheric fissure of each volume was then optimally aligned in the superior-inferior orientation for a precise estimate of the mid-sagittal portion of the CC from each image. The CC was identified in these transformed volumes using an automated labeling procedure developed at the Martinos Center and described in detail previously (Desikan et al., 2006) with an extension to include the CC (Figure 1A). The medial axis (skeleton of the CC was defined on the mid-sagittal slice for the calculation of thickness and DTI measures, based on the approach of Golland and Grimson (Golland et al., 2005) that uses a potential energy field and an elastic force to drive the skeleton into place. This method provides a robust medial axis computation since it is not sensitive to the boundary noise and allows no branching during the skeleton estimation process by representing the skeleton with an undirected graph. The construction of the skeleton is accomplished with an iterative snake-like algorithm using the distance map. The “skeleton” is first initialized as a straight line connecting the genu and splenium and a distance map is created such that the value at each voxel is equal to the minimum distance from the voxel to a point on the CC segmentation border. For points within the CC, the potential energy at each voxel is defined as the magnitude of the gradient of the distance map. For points outside the CC, the potential energy is defined as the negated distance from the nearest boundary point. We next gradually move the skeleton to the ridge of the distance map by moving each point along the gradient of the distance map. In addition, we also add an elastic force to maintain the smoothness of the skeleton. We fix the end points of the initialized skeleton and iterate until the internal points on the skeleton oscillate around the ridge. In the final step, we fix the internal points to re-estimate the skeleton points close to the genu and the splenium and estimate a new reconstruction error. We iterate through all candidate endpoints until a minimum reconstruction error is found. The resulting T1 skeletons consisted of an equal sampling of 200 points along the medial axis (Figure 1B). The thickness of the CC was calculated at each of 200 points along the T1 skeleton, using a threshold cutoff of 0.2, a conservative threshold, to exclude regions outside the callosum, by summing the minimum distance from the skeleton to the superior and inferior boundaries of the segmented CC at each of the 200 points (with the constraint that the angle created between these line segments must be greater than 3.0 radians). This is illustrated in Figure 1C.

DTI pre-processing and analysis. Motion, eddy current and B0 distortion correction—Image pre-processing was performed as described previously (Salat et al., 2005b), using FreeSurfer. First, diffusion volumes were motion corrected and averaged using FLIRT (FMRIB’s Linear Image Registration Tool: http://www.fmrib.ox.ac.uk/

analysis/research/flirt (Jenkinson et al., 2002) with mutual information cost function to first register each average for each direction to the first average of each similar direction and then to register each direction to the T2 weighted DTI volume (no diffusion weighting, the volume with the least eddy current distortion). This motion/eddy current distortion correction procedure performs robustly in registering volumes with different contrast properties and results in a significantly higher signal/contrast to noise volumes compared to averaging without such correction.

Registration of the T1 data to the DTI data: The registration was performed using a novel boundary based registration procedure (BBR) (Greve and Fischl, 2009); this method uses a reference image that is of sufficient resolution and quality to extract surfaces that separate tissue types, in this case, the T1 weighted scans. The input image, in this case DTI, is then aligned to the reference by maximizing the intensity gradient across tissue boundaries. This procedure is particularly suited for this type of cross modal within-participant registration because it takes advantage of anatomical information to co-register images rather than using less anatomically based properties such as the correlation among voxel intensity values. The BBR procedure has been shown to be more accurate than correlation ratios or normalized mutual information and more robust to even strong intensity inhomogeneities (Greve and Fischl, 2009).

Fractional anisotropy (FA) and diffusivity maps calculations: The primary measures acquired from the DTI data were fractional anisotropy, FA, which is a scalar metric that is dependent on the orientational coherence of the diffusion compartments within a voxel and was considered the primary metric of interest (Pierpaoli et al., 2001). The three principal eigenvalues from the diffusion tensor of the DTI data were calculated, representing the diffusion coefficients along the three principal eigenvectors (vectors of diffusion orientation). The CC segmentations were generated automatically using procedures developed at the Martinos Center (Salat et al., 2005b). The mid-sagittal slice of the FA volume was linearly interpolated, and the FA, radial diffusivity and axial diffusivity values were sampled at each of the 200 points along the skeleton. This sampling from the middle voxels of the CC minimized potential contamination of measures from partially volumed voxels at the edges of the CC. Any fornix included in this segmentation was automatically removed. FA was calculated using the standard formula defined previously (Rosas et al., 2006) along each of the 200 points. We additionally examined measures of axial (λ_1) and radial [$(\lambda_2+\lambda_3)/2$] diffusivity as described previously (Song et al., 2002). λ_1 is the largest eigenvalue within a voxel and is presumed to represent the water diffusivity parallel to the majority of axonal fibers. Radial diffusivity represents diffusion perpendicular to the axonal fibers.

Parcellation of the Corpus Callosum: While several schemes for regionally dividing the CC exist (Rajapakse et al., 1996; Witelson, 1989) we adopted Hofer and Frahm’s approach (Hofer and Frahm, 2006), dividing the CC into 5 sub-regions, each believed to subserve distinct functional associations between homologous cortical regions. This method is based on connectional anatomy defined by DTI tractography that is believed less arbitrary than simple proportional division schemes. The five callosal sub-regions were defined as: the anterior sixth (CC1), the anterior half minus the anterior sixth (CC2), the posterior half minus the posterior third (CC3), the posterior third minus the posterior one-fourth (CC4), and the posterior one-fourth (CC5). The intra-class correlation coefficient for intra-rater reliability of the thickness measurements (determined from 4 scans measured 5 times by the same researcher) ranged from 0.99 for CC1 to 0.97 for CC2. These division schemes are illustrated in Figure 1D.

NIH-PA Author Manuscript

NIH-PA Author Manuscript

Statistical Analyses: *HD subjects*: We investigated differences between all HD subjects and controls and we also considered separately differences between HD subjects with TFC above the median TFC (HD1) with all controls, and HD subjects with TFC below the median (HD2) with all controls. We assessed the significance of these group differences using one-way ANOVA models, considering thickness, FA, Radial Diffusivity, Axial Diffusivity in each of the five regions of the CC (CC1, CC2, CC3, CC4 and CC5). For the analyses for high and low TFC's, we used a Bonferroni correction to adjust for multiple comparisons; all results account for multiple comparisons. *PHD subjects*: For PHD subjects and controls, we first compared all subjects to their controls and then divided the PHD subjects into "far" and "near" time to onset (Langbehn et al., 2004). For the first situation, we performed one-way ANOVAs. For the situation where group had three levels (control, near, far), the effect of group in this analysis was in some cases dependent on age and/or sex. Therefore, we used linear regression models with Group as a factor, and Age, Sex and interactions as covariates. We performed multiple comparisons in this regression setting by using the approach of Hothorn et al. (Hothorn et al., 2008), which enabled us to obtain p-values adjusted for multiple comparisons of "near" versus control and "far" versus control over both sexes and over the entire range of Age present in our dataset. Statistical analyses were made using R (Team, 2009), extended with the add-on package "multcomp" of Torston Hothorn (Hothorn et al., 2008). A somewhat more refined spatial investigation of between group differences was performed using point-wise t-tests and Functional Data Analysis techniques (Ramsay and Silverman, 1997). Finally, we examined the association between neuropsychological test results and each of the imaging responses using simple linear regression and Pearson correlations.

RESULTS

Group comparisons: Cross-sectional thickness

The results of the group comparisons are illustrated in Figure 2 and summarized in Table 2. There were no significant differences in the thickness of the CC in PHD subjects when the groups were divided by estimated time to onset. In contrast, in HD subjects, the cross-sectional thickness of the CC and of each one of the CC regions was significantly smaller as compared to controls (CC1 $p < 10^{-6}$, CC2 $p < 0.005$, CC3 $p < 0.01$, CC4 $p < 0.005$, CC5 $p < 0.001$, adjusted for multiple comparisons). Dividing the group further by disease severity did not reveal significant differences between HD1 and HD2 subjects.

We evaluated the magnitude of the thinning as a percentage from measured control values (Table 3). In the group of HD subjects as a whole, CC5, the most posterior region (CC5), was thinned by 24%; CC4 by almost 21%, CC3 by 13%, CC2 by 17% and CC1 by 21%, C2 by 17%. While the magnitude of the thinning was greatest in CC5, there was no significant difference amongst the CC regions nor between the two HD groups. In PHD subjects, reductions in cross-sectional thickness were reduced by approximately 5% in CC3, CC4 and CC5 in the PHD "far" group; in the PHD "near" group, reductions were more substantial: by 8% in CC3, by 14% in CC4 and by 10% in CC5. The distribution of these results recapitulates cortical changes, which have demonstrated thinning of sensori-motor and occipital areas early in disease.

Group Comparisons: Diffusion measures

Fractional Anisotropy: Using a linear regression model which included age and sex as covariates, we found significant reductions in FA in every region of the CC in the PHD group (CC1 $p < 0.95$, CC3 $p < 0.005$, CC3 $p < 0.01$, CC4 $p < 0.05$, CC5 $p < 0.01$). When the group was stratified according to time to estimated onset, significant reductions in FA in the "far" to estimated onset were present only in CC2; in the PHD "near" group, significant reductions were present in CC2, CC3 and CC5 (CC2 $p< 0.001$, CC3p < 0.05, CC5 $p < 0.01$, corrected for multiple comparisons). In HD subjects, FA was significantly lower in all CC regions, ($p < 0.0001$, corrected for multiple comparisons). *Radial Diffusivity*: Radial diffusivity was significantly higher in PHD subjects in CC1, CC2, CC3 and CC5. When the group was stratified by estimated time to onset, radial diffusivity in the "far" group was increased only in regions CC2 and CC5 ($p< 0.05$, $p < 0.001$, respectively, corrected); in the "near" group, radial diffusivity was increase in regions CC2, CC3, and CC5 ($p < 0.005$ for all regions, corrected). Radial diffusivity was significantly increased in all CC regions in HD subjects (CC1 $p < 0.0001$, CC2 $p < 0.005$, CC3 $p < 0.001$, CC4 $p < 10$ -6, CC5 $p < 0.0005$). *Axial Diffusivity*: Axial diffusivity was not significantly different in PHD subjects, either in the group as a whole or when the group was stratified by time to estimated onset. In contrast, in HD subjects, axial diffusivity was increased in every region of the CC (CC1 $p < 0.005$, CC2 $p < 0.05$, CC3 $p < 0.05$, CC4 $p < 0.001$, CC5 $p < 0.05$). Results are summarized in Table 4.

Point-by-Point Comparisons

Thickness and diffusion measures were also calculated along the medial axis skeleton of the corpus callosum at each of 200 points equally spaced along the structure for a point-by-point, more fine-grained, evaluation and are shown in Figure 2b. Using a functional data analysis approach, we found significant thinning extending from points 80 to 165 in PHD subjects closer to expected onset; these points correspond roughly to sub-regions CC3 and CC4, regions that include projections from sensori-motor and parietal cortical regions. The cross-sectional thickness values for both HD1subjects and HD2 subjects were significantly different from controls across each of the 200 points. *FA*: In PHD subjects closer to expected onset, FA values along the entire skeleton were significantly reduced and overlapped with FA values of HD subjects from points 50 to 190, which included portions of CC2, CC3, CC4 and portions of CC5, consistent with the regional analyses. FA values in HD subjects were significantly reduced throughout the entire skeleton as compared to controls, more so in HD2 subjects; however, the differences in FA values were not significantly different between HD1 and HD2 subjects. *Radial Diffusivity*: Radial diffusivity was increased throughout the skeleton in PHD subjects, more so in PHD subjects closer to expected onset, where the curve along points 110 to 150 virtually overlapped with that of HD symptomatic subjects. *Axial Diffusivity*: Axial diffusivity measures were not significantly different from controls in either PHD group; however, there were significant differences in axial diffusivity in HD subjects.

To summarize, changes in diffusion measures, which capture micro-structural changes in the CC in HD were present in subjects more than a decade prior to their expected clinical onset. These alterations appeared to occur in a topologically selective, and temporally predictable, pattern that may reflects early cortical "disconnection". The cross-sectional thickness of the CC was also reduced, but measurable changes were present only in the PHD "near" group, and only in select regions, as well as in the HD group, suggesting that diffusion changes might precede or provide a more sensitive measure of very early pathological change in HD.

Relationship between regional changes in CC and Clinical Measures

We considered whether changes in the CC FA and thickness were associated with performance on the cognitive tasks of the UHDRS. We performed linear regressions to associate performance on the Symbol Digit, Verbal Fluency and Stroop Color Word with FA and CC thickness for every sub-region for PHD and HD subjects, adjusting for age.

We found significant relationships between the Symbol Digit and the FA ($p<0.0001$) and radial diffusivity ($p<0.0001$) with the entire CC, and in the anterior and posterior regions of the CC ($p<0.0001$ in CC1, CC2, and CC5). We also found significant relationships between Verbal Fluency and FA and radial diffusivity of the entire CC ($p<10^{-4}$), and with sub-regions CC1 ($p<10^{-4}$), CC2 ($p<10^{-3}$), and with CC1 ($p<10^{-3}$). We found a significant relationship between Stroop Color Word and radial diffusivity only in CC5 ($p<0.05$). The scatterplots showing these relationships are shown in Figure 3. These findings implicate disrupted inter-hemispheric information transfer in cognitive dysfunction in HD.

There was an association between FA and thickness in HD subjects in all CC regions (R^2 values HD: CC1 0.77, $p < 10^{-5}$, CC2 0.71, $p < 10^{-4}$, CC3 0.60 $p < 0.005$, CC4 0.58 $p < 0.005$, CC5 0.55 $p < 0.01$). However, in PHD subjects this association was present only in CC1 and CC2 (R^2 values PHD: CC1 0. 70, $p < 0.0005$, CC2 0.42, $p < 0.05$), suggesting that FA and thickness may be differentially sensitive to subtle damage and may show associations only after more significant damage is apparent. There was no relationship between normalized caudate volume or CAG repeat number and any of the diffusion measures: FA, radial or axial diffusivity.

DISCUSSION

The principal neurons of the cerebral cortex, pyramidal cells, and their interconnections are the neurologic substrate of many higher order functions such as sensory perception, thought, memory, imagination, emotion, and movement control. These functions are all affected in HD and indeed pyramidal cells have been identified as vulnerable to neurodegeneration. Our understanding from the neuropathology of HD in humans and in genetic animal models is that neurodegeneration is a slow process in which neurons endure prolonged stress-induced alterations that include dendritic and axonal remodeling and retraction that can be expected to alter their connections and functionality long before cell death. Cortical grey matter degeneration has been well documented in HD and recently it has been correlated with important HD symptoms (Rosas et al., 2008a). Pyramidal cell degeneration results in reduction and loss of the complex interconnections these neurons participate in. Loss of local connections likely contributes to cortical thinning and dysfunction. Loss of long connections, many of which are myelinated axons can be predicted in the subcortical white matter as alterations in inter-hemispheric, intra-hemispheric (callosal), and corticofugal pathways. Although atrophy of the subcortical white mater has been described, little is known about its temporal relation to grey matter changes or to clinical features. In this study, we have focused on the corpus callosum because the pyramidal cells giving rise to it are known to be affected early in HD, the topography of projections through it are well understood, and because recent advances in white matter imaging are especially well suited for studying the CC.

The CC is made up primarily from fibers that arise from large pyramidal neurons in layers III and V that give rise to long-reaching intra-cortical projections (Conti and Manzoni, 1994; Innocenti et al., 1995). Here we report early microstructural changes in the CC, as demonstrated by alterations in diffusion measures, including reductions of FA and increases in both axial and radial diffusivity. Reductions in FA typically reflect disruption of white matter microstructure. We found significant reductions of FA in PHD subjects far from expected onset in CC2 and significant reductions in every CC sub-region in PHD subjects close to onset and in HD subjects. In HD, increases in FA could reflect a combination of demyelination and/or degeneration of axons from damaged cortical neurons, decreased density in white matter pathways, breakdown of certain constituents of the cytoskeleton, or decreased directional coherence within the WM pathways (Basser and Pierpaoli, 1996; Salat et al., 2005b; Sehy et al., 2002). We also found significant increases in radial diffusivity, present in CC2 and CC5 in PHD subjects far from expected onset and present in all sub-regions in PHD near and HD subjects. Radial diffusivity measures the perpendicular motion of water in fibers; animal models have suggested that radial diffusivity is sensitive to abnormalities in myelin membranes and may reflect dysmyelination or demyelination (Song et al., 2003). In contrast, we found significant increases in axial diffusivity only in symptomatic HD subjects. Axial diffusivity will increase with increased extra-axonal space, resulting from reduced axonal caliber, which allows faster water molecule movement parallel to axons (Sun et al., 2008). Studies of other neurodegenerative disorders have shown either reductions or increases in these diffusion measures (Salat et al., 2008), each suggesting that these measure may provide early, sensitive measures of neurodegeneration. Significant reduction in the cross-sectional thickness of the CC were also present in HD subjects in all sub-regions; while reductions of more than ten percent were present in the thickness of more posterior CC sub-regions, the reductions in cross-sectional thickness did not reach statistical significance.

These findings are important for several reasons. First, they demonstrate measureable and significant differences in several diffusion measures more than a decade prior to expected clinical symptoms, changes that precede measurable morphometric changes in the CC. Second, they also suggest that alterations in the CC in HD follow both a topologically selective and temporally specific degeneration, with early changes in more posterior segments, primarily those through which fibers from sensori-motor and visual fibers traverse, followed by alterations in more anterior segments. The motor and visual systems are functional systems that are critical early in life and in which myelination occurs early and progresses rapidly (Yakovlev and Lecours, 1967). Both systems are dynamic and are associated with high energetic demands; metabolic dysfunction and alterations in energetics play important mechanistic roles in HD (Beal, 2005; Browne, 2008) and may therefore also contribute to the regional changes in the CC.

Importantly, the temporal and regional patterns of measurable diffusion changes in the CC parallel the pattern of cortical thinning that we have reported previously in HD (Rosas et al., 2008a) and suggest a complex pathophysiology that affects WM and possibly reflects both axonal degeneration and alterations in the characteristics of the myelin sheath (Sotrel et al., 1993). Because changes in diffusion measures were present much earlier than measureable changes in thickness, they may implicate structural alterations and dysfunction of callosal efferent neurons in corresponding regions of cortex prior to frank neurodegeneration. Because few fibers that make up the CC arise from corticostriatal neurons, this work also suggests that cortical degeneration is not dependent on the degeneration of striatal neurons. At the most localized level, these finding may reflect differences in the CC itself and of the specific cortical cells that send fibers through the regions of the CC. As callosal fibers are organized topographically, microstructural changes in either axons or myelin may disrupt the transfer of specific neocortical information across hemispheres and may account for some of the complex cognitive symptoms of HD that have until now been poorly explained by invoking cortico-striatal dysfunction.

The early cognitive and psychiatric symptoms of HD have been the focus of several recent studies; our work suggests that alterations in cortico-cortical connectivity may contribute in a significant way to cognitive dysfunction in HD. We found a significant relationship between cognitive measures and circumscribed reductions in the FA and increases in radial diffusivity of distinct sub-regions, suggesting that disrupted inter-hemispheric information transfer contributes significantly to cognitive dysfunction in HD. Performance on the Verbal Fluency and Symbol digit was associated with these changes in the anterior sub-regions of the CC, consistent with disruptions in fronto-striatal circuitry. We also found an association between diffusion measures in the splenium and the Symbol Digit, perhaps explained by the visuo-spatial demands associated with this task. In contrast, we found no relationship between CC thickness, FA, axial or radial diffusivity and age or CAG repeat length, suggesting that CAG repeat length is likely not a main determinant of CC atrophy in HD.

Summary

We have performed a comprehensive study of the corpus callosum in HD, spanning over 20 years of disease course from remote to distant premanifest to early symptomatic disease. Our results demonstrate that the corpus callosum develops regionally selective changes in its microstructural anatomy early in HD, more than a decade before the onset of motor symptoms. These alterations occur prior to measurable atrophy and likely reflect degeneration of callosal projecting pyramidal neurons in the neocortex, loss of cortico-cortical connectivity, and functional compromise of associative cortical processing. The result is a significant contribution to the cognitive deficits of HD. Our results reaffirm the clinical and pathophysiological importance of the cortex and altered cortical circuitry and function in HD and suggest a role for progressive WM alterations in the clinical symptoms that occur.

Acknowledgments

Supported for this research was provided by in part by NIH NS042861, NI058793, NIH K01AG024898, R01NR010827, the Athinoula A. Martinos Foundation, the High Q Foundation, the National Center for Research Resources (P41-RR14075, R01 RR16594-01A1 and the NCRR BIRN Morphometric Project BIRN002, U24 RR021382), the National Institute for Biomedical Imaging and Bioengineering (R01 EB001550), the National Institute for Neurological Disorders and Stroke (R01 NS052585), the National Institute on Aging (AG02238) as well as the Mental Illness and Neuroscience Discovery (MIND) Institute, and is part of the National Alliance for Medical Image Computing (NAMIC), funded by the National Institutes of Health through the NIH Roadmap. We are especially grateful to the New England HDSA Center of Excellence and its patients, who so generously contributed to this work.

References

Basser PJ, Pierpaoli C. Microstructural and physiological features of tissues elucidated by quantitative-diffusion-tensor MRI. J Magn Reson B. 1996; 111:209–219. [PubMed: 8661285]

Beal MF. Mitochondria take center stage in aging and neurodegeneration. Ann Neurol. 2005; 58:495–505. [PubMed: 16178023]

Browne SE. Mitochondria and Huntington's disease pathogenesis: insight from genetic and chemical models. Ann N Y Acad Sci. 2008; 1147:358–382. [PubMed: 19076457]

Budde MD, Kim JH, Liang HF, Schmidt RE, Russell JH, Cross AH, Song SK. Toward accurate diagnosis of white matter pathology using diffusion tensor imaging. Magn Reson Med. 2007; 57:688–695. [PubMed: 17390365]

Cercignani M, Horsfield MA. The physical basis of diffusion-weighted MRI. J Neurol Sci. 2001; 186(Suppl 1):S11–14. [PubMed: 11334985]

Conti F, Manzoni T. The neurotransmitters and postsynaptic actions of callosally projecting neurons. Behav Brain Res. 1994; 64:37–53. [PubMed: 7840891]

Desikan RS, Segonne F, Fischl B, Quinn BT, Dickerson BC, Blacker D, Buckner RL, Dale AM, Maguire RP, Hyman BT, Albert MS, Killiany RJ. An automated labeling system for subdividing the human cerebral cortex on MRI scans into gyral based regions of interest. Neuroimage. 2006; 31:968–980. [PubMed: 16530430]

Douaud G, Behrens TE, Poupon C, Cointepas Y, Jbabdi S, Gaura V, Golestani N, Krystkowiak P, Verny C, Damier P, Bachoud-Levi AC, Hantraye P, Remy P. In vivo evidence for the selective subcortical degeneration in Huntington's disease. Neuroimage. 2009; 46:958–966. [PubMed: 19332141]

Golland P, Grimson WE, Shenton ME, Kikinis R. Detection and analysis of statistical differences in anatomical shape. Med Image Anal. 2005; 9:69–86. [PubMed: 15581813]

Greve DN, Fischl B. Accurate and robust brain image alignment using boundary-based registration. Neuroimage. 2009

Hedreen JC, Peyser CE, Folstein SE, Ross CA. Neuronal loss in layers V and VI of cerebral cortex in Huntington's disease. Neurosci Lett. 1991; 133:257–261. [PubMed: 1840078]

Hofer S, Frahm J. Topography of the human corpus callosum revisited--comprehensive fiber tractography using diffusion tensor magnetic resonance imaging. Neuroimage. 2006; 32:989–994. [PubMed: 16854598]

Hothorn T, Bretz F, Westfall P. Simultaneous inference in general parametric models. Biom J. 2008; 50:346–363. [PubMed: 18481363]

Innocenti GM. Some new trends in the study of the corpus callosum. Behav Brain Res. 1994; 64:1–8. [PubMed: 7840876]

Innocenti GM, Aggoun-Zouaoui D, Lehmann P. Cellular aspects of callosal connections and their development. Neuropsychologia. 1995; 33:961–987. [PubMed: 8524456]

Jenkinson M, Bannister P, Brady M, Smith S. Improved optimization for the robust and accurate linear registration and motion correction of brain images. Neuroimage. 2002; 17:825–841. [PubMed: 12377157]

Jones DK, Horsfield MA, Simmons A. Optimal strategies for measuring diffusion in anisotropic systems by magnetic resonance imaging. Magn Reson Med. 1999; 42:515–525. [PubMed: 10467296]

Keshavan MS, Diwadkar VA, Harenski K, Rosenberg DR, Sweeney JA, Pettegrew JW. Abnormalities of the corpus callosum in first episode, treatment naive schizophrenia. J Neurol Neurosurg Psychiatry. 2002; 72:757–760. [PubMed: 12023420]

Kim EY, Park HJ, Kim DH, Lee SK, Kim J. Measuring fractional anisotropy of the corpus callosum using diffusion tensor imaging: mid-sagittal versus axial imaging planes. Korean J Radiol. 2008; 9:391–395. [PubMed: 18838846]

Kim JH, Budde MD, Liang HF, Klein RS, Russell JH, Cross AH, Song SK. Detecting axon damage in spinal cord from a mouse model of multiple sclerosis. Neurobiol Dis. 2006; 21:626–632. [PubMed: 16298135]

Kloppel S, Draganski B, Golding CV, Chu C, Nagy Z, Cook PA, Hicks SL, Kennard C, Alexander DC, Parker GJ, Tabrizi SJ, Frackowiak RS. White matter connections reflect changes in voluntary-guided saccades in pre-symptomatic Huntington's disease. Brain. 2008; 131:196–204. [PubMed: 18056161]

Langbehn DR, Brinkman RR, Falush D, Paulsen JS, Hayden MR. A new model for prediction of the age of onset and penetrance for Huntington's disease based on CAG length. Clin Genet. 2004; 65:267–277. [PubMed: 15025718]

Lange H, Thorner G, Hopf A, Schroder KF. Morphometric studies of the neuropathological changes in choreatic diseases. J Neurol Sci. 1976; 28:401–425. [PubMed: 133209]

Lowe MJ, Horenstein C, Hirsch JG, Marrie RA, Stone L, Bhattacharyya PK, Gass A, Phillips MD. Functional pathway-defined MRI diffusion measures reveal increased transverse diffusivity of water in multiple sclerosis. Neuroimage. 2006; 32:1127–1133. [PubMed: 16798013]

Pfefferbaum A, Adalsteinsson E, Rohlfing T, Sullivan EV. Diffusion tensor imaging of deep gray matter brain structures: Effects of age and iron concentration. Neurobiol Aging. 2008

Pierpaoli C, Barnett A, Pajevic S, Chen R, Penix LR, Virta A, Basser P. Water diffusion changes in Wallerian degeneration and their dependence on white matter architecture. Neuroimage. 2001; 13:1174–1185. [PubMed: 11352623]

Rajapakse JC, Giedd JN, Rumsey JM, Vaituzis AC, Hamburger SD, Rapoport JL. Regional MRI measurements of the corpus callosum: a methodological and developmental study. Brain Dev. 1996; 18:379–388. [PubMed: 8891233]

Ramsay, J.; Silverman, BW. Functional Data Analysis. 2. Springer; 1997.

Reading SA, Yassa MA, Bakker A, Dziorny AC, Gourley LM, Yallapragada V, Rosenblatt A, Margolis RL, Aylward EH, Brandt J, Mori S, van Zijl P, Bassett SS, Ross CA. Regional white matter change in pre-symptomatic Huntington's disease: a diffusion tensor imaging study. Psychiatry Res. 2005; 140:55–62. [PubMed: 16199141]

Reese TG, Heid O, Weisskoff RM, Wedeen VJ. Reduction of eddy-current-induced distortion in diffusion MRI using a twice-refocused spin echo. Magn Reson Med. 2003; 49:177–182. [PubMed: 12509835]

Rosas HD, Liu AK, Hersch S, Glessner M, Ferrante RJ, Salat DH, van der Kouwe A, Jenkins BG, Dale AM, Fischl B. Regional and progressive thinning of the cortical ribbon in Huntington's disease. Neurology. 2002; 58:695–701. [PubMed: 11889230]

Rosas HD, Salat DH, Lee SY, Zaleta AK, Hevelone N, Hersch SM. Complexity and heterogeneity: what drives the ever-changing brain in Huntington's disease? Ann N Y Acad Sci. 2008a; 1147:196–205. [PubMed: 19076442]

Rosas HD, Salat DH, Lee SY, Zaleta AK, Pappu V, Fischl B, Greve D, Hevelone N, Hersch SM. Cerebral cortex and the clinical expression of Huntington's disease: complexity and heterogeneity. Brain. 2008b; 131:1057–1068. [PubMed: 18337273]

Rosas HD, Tuch DS, Hevelone ND, Zaleta AK, Vangel M, Hersch SM, Salat DH. Diffusion tensor imaging in presymptomatic and early Huntington's disease: Selective white matter pathology and its relationship to clinical measures. Mov Disord. 2006; 21:1317–1325. [PubMed: 16755582]

Sach M, Winkler G, Glauche V, Liepert J, Heimbach B, Koch MA, Buchel C, Weiller C. Diffusion tensor MRI of early upper motor neuron involvement in amyotrophic lateral sclerosis. Brain. 2004; 127:340–350. [PubMed: 14607785]

Salat DH, Tuch DS, Greve DN, van der Kouwe AJ, Hevelone ND, Zaleta AK, Rosen BR, Fischl B, Corkin S, Rosas HD, Dale AM. Age-related alterations in white matter microstructure measured by diffusion tensor imaging. Neurobiol Aging. 2005a; 26:1215–1227. [PubMed: 15917106]

Salat DH, Tuch DS, Hevelone ND, Fischl B, Corkin S, Rosas HD, Dale AM. Age-related changes in prefrontal white matter measured by diffusion tensor imaging. Ann N Y Acad Sci. 2005b; 1064:37–49. [PubMed: 16394146]

Salat DH, Tuch DS, van der Kouwe AJ, Greve DN, Pappu V, Lee SY, Hevelone ND, Zaleta AK, Growdon JH, Corkin S, Fischl B, Rosas HD. White matter pathology isolates the hippocampal formation in Alzheimer's disease. Neurobiol Aging. 2008

Schulte T, Sullivan EV, Muller-Oehring EM, Adalsteinsson E, Pfefferbaum A. Corpus callosal microstructural integrity influences interhemispheric processing: a diffusion tensor imaging study. Cereb Cortex. 2005; 15:1384–1392. [PubMed: 15635059]

Sehy JV, Banks AA, Ackerman JJ, Neil JJ. Importance of intracellular water apparent diffusion to the measurement of membrane permeability. Biophys J. 2002; 83:2856–2863. [PubMed: 12414717]

Song SK, Sun SW, Ju WK, Lin SJ, Cross AH, Neufeld AH. Diffusion tensor imaging detects and differentiates axon and myelin degeneration in mouse optic nerve after retinal ischemia. Neuroimage. 2003; 20:1714–1722. [PubMed: 14642481]

Song SK, Sun SW, Ramsbottom MJ, Chang C, Russell J, Cross AH. Dysmyelination revealed through MRI as increased radial (but unchanged axial) diffusion of water. Neuroimage. 2002; 17:1429–1436. [PubMed: 12414282]

Song SK, Yoshino J, Le TQ, Lin SJ, Sun SW, Cross AH, Armstrong RC. Demyelination increases radial diffusivity in corpus callosum of mouse brain. Neuroimage. 2005; 26:132–140. [PubMed: 15862213]

Sotrel A, Williams RS, Kaufmann WE, Myers RH. Evidence for neuronal degeneration and dendritic plasticity in cortical pyramidal neurons of Huntington's disease: a quantitative Golgi study. Neurology. 1993; 43:2088–2096. [PubMed: 8413971]

Stricker NH, Schweinsburg BC, Delano-Wood L, Wierenga CE, Bangen KJ, Haaland KY, Frank LR, Salmon DP, Bondi MW. Decreased white matter integrity in late-myelinating fiber pathways in Alzheimer's disease supports retrogenesis. Neuroimage. 2009; 45:10–16. [PubMed: 19100839]

Sullivan EV, Pfefferbaum A. Diffusion tensor imaging and aging. Neurosci Biobehav Rev. 2006; 30:749–761. [PubMed: 16887187]

Sun SW, Liang HF, Cross AH, Song SK. Evolving Wallerian degeneration after transient retinal ischemia in mice characterized by diffusion tensor imaging. Neuroimage. 2008; 40:1–10. [PubMed: 18187343]

Sun SW, Liang HF, Le TQ, Armstrong RC, Cross AH, Song SK. Differential sensitivity of in vivo and ex vivo diffusion tensor imaging to evolving optic nerve injury in mice with retinal ischemia. Neuroimage. 2006; 32:1195–1204. [PubMed: 16797189]

Sun SW, Neil JJ, Song SK. Relative indices of water diffusion anisotropy are equivalent in live and formalin-fixed mouse brains. Magn Reson Med. 2003; 50:743–748. [PubMed: 14523960]

NIH-PA Author Manuscript

NIH-PA Author Manuscript

Team R-DC. R: A Language and Environment for Statistical Computing. 2009

Weaver KE, Richards TL, Liang O, Laurino MY, Samii A, Aylward EH. Longitudinal diffusion tensor imaging in Huntington's Disease. Exp Neurol. 2009; 216:525–529. [PubMed: 19320010]

Witelson SF. Hand and sex differences in the isthmus and genu of the human corpus callosum. A postmortem morphological study. Brain. 1989; 112(Pt 3):799–835. [PubMed: 2731030]

Yakovlev, PI.; Lecours, AR. The myelogenetic cycles of regional maturation of the brain. In: Minkowski, A., editor. Regional Development of the Brain in Early Life. F.A. Davis Company; Philadelphia: 1967. p. 3-70.

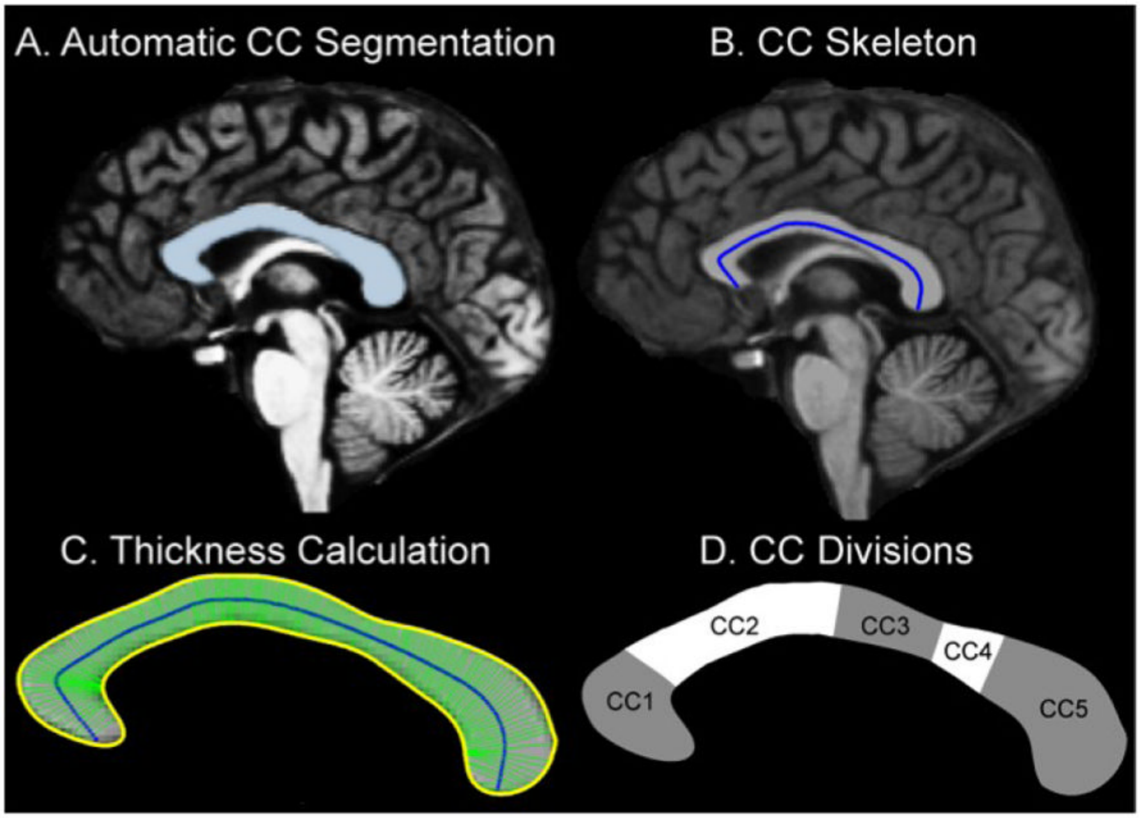

Figure 1. Corpus Callosum Segmentation

1A. *Segmentation of the Corpus Callosum*. The CC was identified in the transformed volume using an automated labeling procedure developed at the Martinos Center. **1B**. *CC Skeleton*. A"skeleton" was generated by creating a line connecting the genu and the splenium such that the value of each voxel making up this line was equal to the minimum distance from the voxel to a point on the CC segmentation border. **1C**. *CC Thickness*. The thickness at each of the 200 points along the skeleton was estimated as the distance between the superior and inferior borders with the constraint that the angle between these was greater than 3.0 radians. **1D**.*Topography of the midsaggital corpus callosum and proposed fiber composition, based on Hofer and Frahm's classification*. CC1 prefrontal, CC2 Premotor and supplementary motor, CC3-CC4 sensori-motor, CC5: parietal, temporal and occipital.

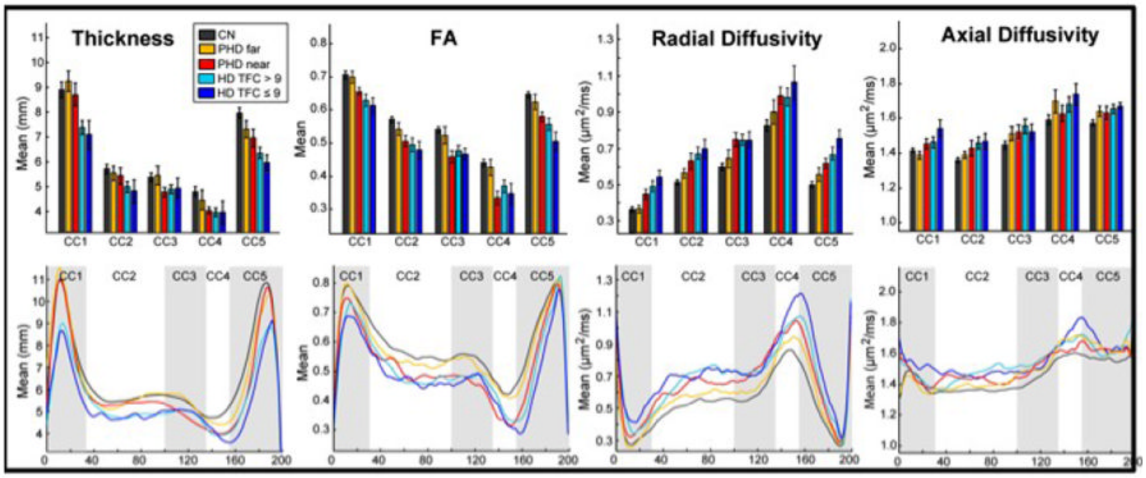

Figure 2. Summary of Diffusion Alterations in HD

Boxplots of thickness, FA, Radial Diffusivity, and Axial Diffusivity measures. Significant reductions in cross-sectional thickness of each of the CC parcellations were present in symptomatic HD (CC1 $p < 10^{-6}$, CC2 $p < 0.005$, CC3 $p < 0.01$, CC4 $p < 0.005$, CC5 $p < 0.001$, corrected) but not PHD subjects. Significant reductions in FA (CC1 $p < 0.95$, CC3 $p < 0.005$, CC3 $p < 0.01$, CC4 $p < 0.05$, CC5 $p < 0.01$, corrected) and increases in radial (“far” group: regions CC2 $p< 0.05$and CC5 $p < 0.001$; “near” :CC2, CC3, and CC5, $p < 0.005$ for all regions; HD: CC1 $p < 0.0001$, CC2 $p < 0.005$, CC3 $p < 0.001$, CC4 $p < 10$ -6, CC5 $p < 0.0005$, corrected) and axial diffusivity in HD subjects (CC1 $p < 0.005$, CC2 $p < 0.05$, CC3 $p < 0.05$, CC4 $p < 0.001$, CC5 $p < 0.05$, corrected) were present. The point-by-point plots suggest that diffusion changes may precede measureable morphometric changes. The differences in the magnitude of the effects supports a topographically distinct pattern of CC degeneration.

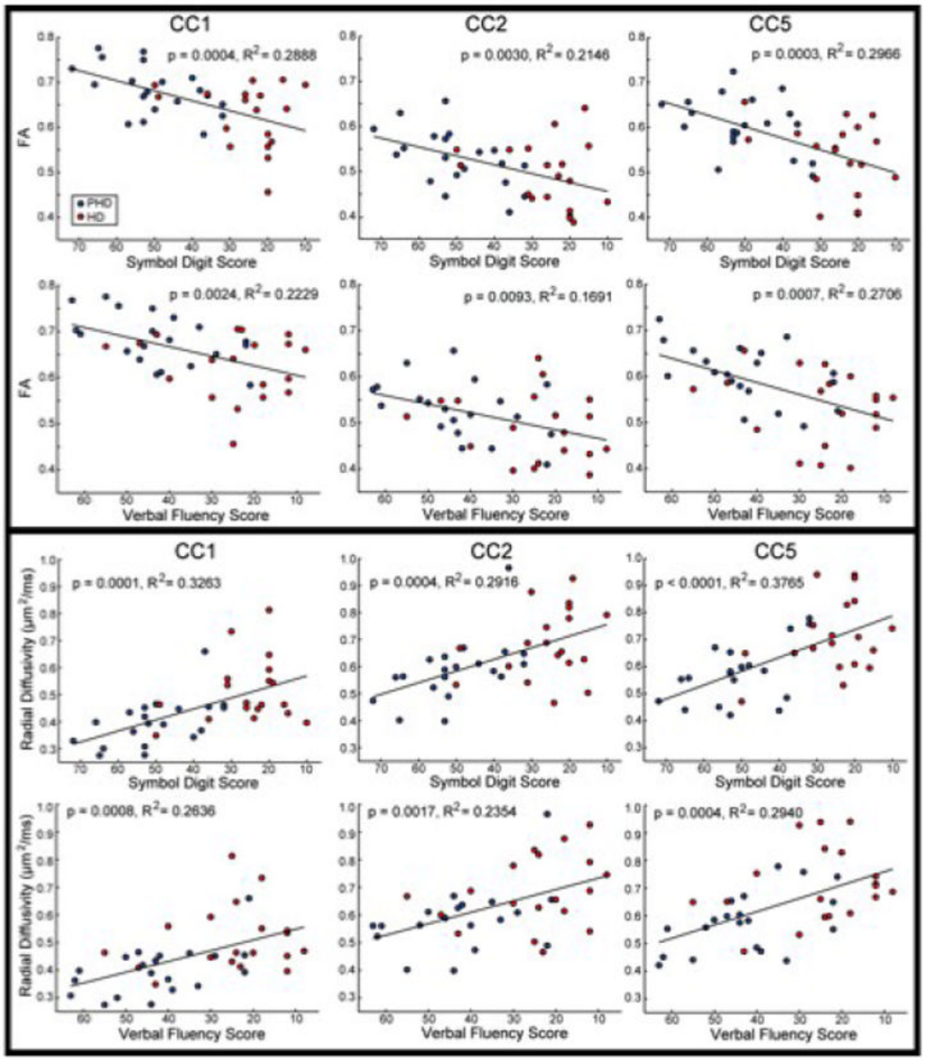

Figure 3. Scatter plots demonstrating the correlation between diffusion parameters and clinical measures

The scatter plots demonstrate a significant relationship between regional FA and radial diffusivity and performance on the Verbal Fluency and Symbol Digit Scores, with significant correlations in CC1, CC2 and CC5, further supporting an important role of the cortex in cognitive dysfunction in HD.

Table 1

Demographic and clinical data of study subjects

	PHD-controls (N=21)	PHD Group (N=21)	PHD "far" (N=11)	PHD "near" (N=10)	HD-controls (N=19)	HD Group (N=21)	HD1 (N=13)	HD2 (N=8)
Age	39.7± 11.3	40.2 ± 10.4	32.6 ± 5.0	47.0 ± 9.7	45.2 ± 8.7	46.5 ± 9.3	46.4 ± 8.9	46.4 ± 8.9
Sex	8M/13F	12M/7F	5M/6F	3M/7F	7M/12F	8M/13F	5M/8F	3M/5F
CAG repeat*	N/A	42.4 ± 2.7	41.7± 2.2	43.4 ± 3.2	N/A	44.8 ± 2.4	44.6 +/- 2.7	45.3 +/- 1.6
TFC**	13 ± 0	12.9 ± 0.3	12.9 ± 0.3	12.9 ± 0.4	13 ± 0	9.6 ± 2.4	10.4 ± 0.8	8.25 ± 0.9
Verbal Fluency	41.9 ± 8.9	42.5 ± 12.8	46.2 ± 10.2	37.0 ± 14.3	43.6 ± 10.0	25.2 ± 13.1	29.9 ± 14.7	18.6 ± 6.6
Stroop	45.3 ± 6.4	43.0 ± 8.8	45.7 ± 9.5	39.6 ± 7.8	46.4 ± 3.7	27.8 ± 11.4	30.5 ± 13.4	24.3 ± 7.4
Symbol Digit	62.5 ± 8.6	50.1 ± 11.7	52.5 ± 11.3	45.7 ± 11.1	58.9 ± 9.0	25.7 ± 10.5	27.9 ± 12.3	22.6 ± 6.7

*Missing CAG data for 2 HD subjects.

**Missing TFC scores for 3 PHD

***Missing UHDRS scores for 2 controls, 1 PHD subject and 2 HD subjects

NIH-PA Author Manuscript

NIH-PA Author Manuscript

Table 2

Cross-sectional thickness of the CC and its sub-regions.

	PHD controls (N=21)	PHD subjects (N=21)	PHD “far” (N=11)	PHD “near” (N10)	HD controls (N=19)	HD subjects (N=21)	HD1 (N=13)	HD2 (N=8)
CC1	8.86 ± 1.80	8.90 ± 1.38	9.26 ± 1.31	8.71 ± 1.41	9.24 ± 1.63	7.28 ± 1.24††	7.38 ± 1.02†	7.11 ± 1.61††
CC2	5.61 ± 0.95	5.56 ± 0.92	5.55 ± 0.93	5.44 ± 0.94	5.97 ± 0.89	4.93 ± 1.00**	5.00 ± 0.81*	4.83 ± 1.30#
CC3	5.24 ± 0.92	5.19 ± 0.99	5.47 ± 1.23	4.79 ± 0.61	5.70 ± 0.81	4.93 ± 0.84*	4.91 ± 0.67*	4.96 ± 1.11*
CC4	4.70 ± 0.89	4.28 ± 0.89	4.47 ± 1.23	4.05 ± 0.39	5.02 ± 1.05	3.99 ± 0.91**	3.99 ± 0.63*	3.98 ± 1.31*
CC5	7.74 ± 1.04	7.14 ± 1.03	7.33 ± 1.11	6.96 ± 1.07	8.23 ± 1.01	6.22 ± 0.84***	6.36 ± 0.82**	5.97 ± 0.86*

Data are presented at mean ± SD of the total thickness in millimeters in each of 5 sub-regions (CC1 to CC5, anterior to posterior).

Significant at

†† $p < 10^{-6}$,

† $p<10^{-5}$

*** $p < 0.001$,

** $p < 0.005$;

* $p<0.01$,

\# $p < 0.05$ corrected for multiple comparisons as described in text.

NIH-PA Author Manuscript
NIH-PA Author Manuscript

Table 3

Percent Reductions in Cross-sectional thickness of CC sub-regions.

Region	PHD Group(N=21)	PHD "far" (N=11)	PHD "near" (N=10)	HD Group (N=21)	HD1 (N=13)	HD2 (N=8)
CC1	-0.47%	-0.54%	1.65%	21.25%	20.1%	23.1%
CC2	0.97%	1.16%	3.03%	17.40%	16.2%	19.1%
CC3	0.97%	-4.23%	8.63%	13.45%	13.8%	13.0%
CC4	8.86%	4.85%	13.81%	20.64%	20.5%	20.5%
CC5	7.77%	5.34%	10.06%	24.44%	22.7%	27.5%

Table 4

Corpus Callosum DTI measures: FA, Axial Diffusivity, Radial Diffusivity

	Region	PHD- controls (N=21)	PHD "far" (N=11)	PHD "near" (N=10)	HD controls (N=19)	HD1 (N=13)	HD2 (N=8)
FA	***Whole***	0.59 ± 0.039	0.57 ± 0.056	0.52 ± 0.033 *	0.60 ± 0.038	0.51 ± 0.060 ***	0.49 ± 0.061 **
	CC						
	CC1	0.72 ± 0.058	0.70 ± 0.057	0.66 ± 0.036 *	0.70 ± 0.059	0.63 ± 0.067 ***	0.61 ± 0.068 ††
	CC2	0.57 ± 0.050	0.54 ± 0.063 ***	0.51 ± 0.054 ***	0.58 ± 0.041	0.49 ± 0.075 ***	0.48 ± 0.073 †
	CC3	0.53 ± 0.053	0.52 ± 0.081	0.46 ± 0.053 *	0.55 ± 0.049	0.48 ± 0.055 ***	0.47 ± 0.051 ††
	CC4	0.44 ± 0.062	0.43 ± 0.075	0.33 ± 0.065 *	0.45 ± 0.063	0.37 ± 0.072 †	0.35 ± 0.089 ††
	CC5	0.65 ± 0.047	0.62 ± 0.072	0.58 ± 0.044 ***	0.64 ± 0.048	0.56 ± 0.066 ***	0.51 ± 0.078 †
Axial	***Whole***	1.47 ± 0.078	1.50 ± 0.078	1.51 ± 0.108	1.44 ± 0.062	1.54 ± 0.105 **	1.56 ± 0.095 **
	CC						
	CC1	1.42 ± 0.059	1.39 ± 0.069	1.46 ± 0.087	1.42 ± 0.075	1.46 ± 0.113 *	1.54 ± 0.130 **
	CC2	1.37 ± 0.086	1.39 ± 0.067	1.43 ± 0.139	1.34 ± 0.056	1.46 ± 0.128	1.47 ± 0.127 *
	CC3	1.46 ± 0.117	1.51 ± 0.127	1.52 ± 0.118	1.43 ± 0.099	1.56 ± 0.151 *	1.52 ± 0.126 *
	CC4	1.60 ± 0.164	1.70 ± 0.209	1.63 ± 0.139	1.57 ± 0.146	1.68 ± 0.153 ***	1.74 ± 0.176 ***
	CC5	1.58 ± 0.106	1.64 ± 0.092	1.63 ± 0.118	1.57 ± 0.081	1.65 ± 0.099 ***	1.67 ± 0.057 ***
Radial	***Whole***	0.54 ± 0.073	0.58 ± 0.094	0.66 ± 0.081 *	0.52 ± 0.058	0.69 ± 0.106 ***	0.73 ± 0.130 **
	CC						
	CC1	0.35 ± 0.067	0.37 ± 0.068	0.45 ± 0.085 *	0.36 ± 0.064	0.49 ± 0.111 ††	0.54 ± 0.117 ††
	CC2	0.52 ± 0.088	0.56 ± 0.082 *	0.63 ± 0.134 ***	0.49 ± 0.054	0.67 ± 0.120 ***	0.70 ± 0.145 ***
	CC3	0.61 ± 0.095	0.64 ± 0.150	0.75 ± 0.113 ***	0.57 ± 0.086	0.74 ± 0.115 ††	0.75 ± 0.125 ***
	CC4	0.84 ± 0.172	0.90 ± 0.213	0.99 ± 0.137	0.79 ± 0.151	0.98 ± 0.178 ††	1.06 ± 0.265 ††
	CC5	0.50 ± 0.080	0.56 ± 0.114 ***	0.62 ± 0.091 ***	0.50 ± 0.071	0.67 ± 0.126 †	0.76 ± 0.135 ††

* $p<0.05$,

** $p<0.01$,

*** $p < 0.005$,

NIH-PA Author Manuscript

NIH-PA Author Manuscript

† $p < 0.0005$,

†† $p < 0.0001$ corrected for multiple comparisons. Axial and Radial diffusivity are given in $\mu m^2/ms$. Fractional anisotropy is without units.